Energy dynamics in a simulation of LAPD turbulence

B. Friedman,[1, a)] T.A. Carter,[1] M.V. Umansky,[2] D. Schaffner,[1] and B. Dudson[3]

[1)] *Department of Physics and Astronomy, University of California, Los Angeles, California 90095-1547, USA*

[2)] *Lawrence Livermore National Laboratory, Livermore, California 94550, USA*

[3)] *Department of Physics, University of York, Heslington, York YO10 5DD, United Kingdom*

Energy dynamics calculations in a 3D fluid simulation of drift wave turbulence in the linear Large Plasma Device (LAPD) [W. Gekelman *et al.*, Rev. Sci. Inst. **62**, 2875 (1991)] illuminate processes that drive and dissipate the turbulence. These calculations reveal that a nonlinear instability dominates the injection of energy into the turbulence by overtaking the linear drift wave instability that dominates when fluctuations about the equilibrium are small. The nonlinear instability drives flute-like ($k_\parallel = 0$) density fluctuations using free energy from the background density gradient. Through nonlinear axial wavenumber transfer to $k_\parallel \neq 0$ fluctuations, the nonlinear instability accesses the adiabatic response, which provides the requisite energy transfer channel from density to potential fluctuations as well as the phase shift that causes instability. The turbulence characteristics in the simulations agree remarkably well with experiment. When the nonlinear instability is artificially removed from the system through suppressing $k_\parallel = 0$ modes, the turbulence develops a coherent frequency spectrum which is inconsistent with experimental data.

[a)] Electronic mail: friedman@physics.ucla.edu

I. INTRODUCTION

It is common practice to study a system's linear stability properties to gain insight into turbulent dynamics. It is often easier to calculate and analyze linear modes and growth rates than to simulate and analyze nonlinear turbulence. However, there are several situations in which linear properties can be misleading in understanding turbulent systems. First, linear studies of magnetically confined plasmas that neglect stable branches of the linear dispersion relation often miss details of nonlinear dynamics. For example, stable eigenmodes can often impact nonlinear dynamics by providing energy sinks and sometimes energy sources not found on the most unstable linear branch[1–10]. Stable eigenmodes can shift the energy injection and dissipation ranges, making the turbulent dynamics very different from the Kolmogorov picture of hydrodynamic turbulence[11]. Second, systems with non-normal modes (non-orthogonal eigenvectors) display properties that are unexpected from linear calculations[12]. In fact, systems with non-normal modes even make it difficult to predict dynamics when stable eigenmode branches are included in analyses[8]. Third, linear stability analysis can miss crucial nonlinear instability effects, which come in several varieties.

The most obvious variety of a nonlinear instability effect is that of subcritical turbulence in which no linear instabilities exist but turbulence is self-sustained given finite-amplitude seed perturbations. Subcritical turbulence is common in hydrodynamics[13]. While not as well-known in plasma physics, several cases of subcritical plasma instabilities have been shown in the literature[14–20]. The second variety of nonlinear instability includes cases in which a particular linear instability is present in a system, but the turbulence is maintained by a nonlinear instability mechanism with different physical origin than the linear instability mechanism. This has been explored in tokamak edge simulations in which linear ballooning instability drive is overtaken in the saturated phase by a nonlinear drift-wave drive[21–25]. Finally, it is often found that a particular linear instability is enhanced, depressed, and/or modified in the saturated phase by a nonlinear instability with a similar mechanism as the linear instability. In some of these cases nonlinear wavenumber transfers can increase or cause drive[26,27], while in other cases zonal flow effects decrease drive[28,29].

In order to avoid the pitfalls of relying too heavily on linear stability calculations in forming conclusions on turbulence characteristics, it is useful to perform turbulent simulations and diagnose them with energy dynamics analyses. Energy dynamics analyses track energy

input into turbulent fluctuations and energy dissipation out of them. They also track conservative energy transfer between different energy types (e.g. from potential to kinetic energy) and between different scales, waves, or eigenmodes of a system. In all, energy dynamics analysis can be used as a post-processing tool to characterize simulation turbulence in order to gain insight into underlying physical processes.

In this study, a simulation of a two-fluid Braginskii model of turbulence in the Large Plasma Device (LAPD) is subjected to such an energy dynamics analysis. This reveals that a nonlinear instability drives and maintains the turbulence in the steady state saturated phase of the simulation. While a linear resistive drift wave instability resides in the system, the nonlinear drift wave instability dominates when the fluctuation amplitude is over a few percent of the equilibrium value. The primary linear instability is the resistive drift wave which has a positive linear growth rate for low but finite $k_\parallel$. However, the saturated state of the simulated turbulence is strongly dominated by flute-like ($k_\parallel = 0$) fluctuations in density and potential. The flute-like fluctuation spectrum is generated by a nonlinear instability. The nonlinear instability is identified by its energy growth rate spectrum, which varies significantly from the linear growth rate spectrum. If $k_\parallel = 0$ fluctuations are removed from the simulation (while retaining zonal flows), the saturated turbulent state is qualitatively and quantitatively different and much less consistent with experimental measurement.

II. THE DRIFT WAVE MODEL

A Braginskii-based fluid model[30] is used to simulate drift wave turbulence in LAPD using the BOUT++ code[31]. The evolved variables in the model are the plasma density, N, the electron fluid parallel velocity $v_{\parallel e}$, the potential vorticity $\varpi \equiv \nabla_\perp \cdot (N_0 \nabla_\perp \phi)$, and the electron temperature T_e. The ions are assumed cold in the model ($T_i = 0$), which eliminates ion temperature gradient drive, and sound wave effects are neglected. Details of the simulation code and derivations of the model may be found in previous LAPD verification and validation studies[32–35], although electron temperature fluctuations were not included in those studies.

The equations are developed with Bohm normalizations: lengths are normalized to the ion sound gyroradius ρ_s, times to the ion cyclotron time ω_{ci}^{-1}, velocities to the sound speed c_s, densities to the equilibrium peak density, and electron temperatures and potentials to

the equilibrium peak electron temperature. All of these values are constants (not functions of radius) and the physical quantities used to calculate these constants are the following: the magnetic field is 1 kG, the ion unit mass is 4, the peak density is 2.86×10^{12} cm^{-3}, and the peak electron temperature is 6 eV. The equations are:

$$\partial_t N = -\mathbf{v}_E \cdot \nabla N_0 - N_0 \nabla_\parallel v_{\parallel e} + \mu_N \nabla_\perp^2 N + S_N + \{\phi, N\}, \tag{1}$$

$$\partial_t v_{\parallel e} = -\frac{m_i}{m_e}\frac{T_{e0}}{N_0}\nabla_\parallel N - 1.71\frac{m_i}{m_e}\nabla_\parallel T_e + \frac{m_i}{m_e}\nabla_\parallel \phi - \nu_e v_{\parallel e} + \{\phi, v_{\parallel e}\}, \tag{2}$$

$$\partial_t \varpi = -N_0 \nabla_\parallel v_{\parallel e} - \nu_{in}\varpi + \mu_\phi \nabla_\perp^2 \varpi + \{\phi, \varpi\}, \tag{3}$$

$$\partial_t T_e = -\mathbf{v}_E \cdot \nabla T_{e0} - 1.71\frac{2}{3}T_{e0}\nabla_\parallel v_{\parallel e} + \frac{2}{3N_0}\kappa_{\parallel e}\nabla_\parallel^2 T_e - \frac{2m_e}{m_i}\nu_e T_e + \mu_T \nabla_\perp^2 T_e + S_T + \{\phi, T_e\}. \tag{4}$$

In these equations, μ_N, μ_T, and μ_ϕ are artificial diffusion and viscosity coefficients used for sub-grid dissipation. They are large enough to allow saturation and grid convergence[35], but small enough to allow for turbulence to develop. In the simulations, they are all given the same value of 1.25×10^{-3} in Bohm-normalized units. This is the only free parameter in the simulations. All other parameters such as the electron collisionality ν_e, ion-neutral collisionality ν_{in}, parallel electron thermal conductivity $\kappa_{\parallel e}$, and mass ratio $\frac{m_i}{m_e}$ are calculated from the experimental parameters. There are two sources of free energy: the density gradient due to the equilibrium density profile N_0, and the equilibrium electron temperature gradient in T_{e0}, both of which are taken from experimental fits. N_0 and T_{e0} are functions of only the radial cylindrical coordinate r, and they are shown in Fig. 1.

The terms in Poisson brackets are the $E \times B$ advective nonlinearities, which are the only nonlinearities used in the simulations. The numerical simulations are fully spatial in all three dimensions (as opposed to spectral) and use cylindrical annular geometry ($12 < r < 40$ cm). The radial extent used in the simulation encompasses the region where fluctuations are above a few percent in the experiment. The simulations use periodic boundary conditions in the axial (z) direction and Dirichlet boundary conditions in the radial (r) direction for the fluctuating quantities.

Simulations also use density and temperature sources (S_n and S_T) in order to keep the equilibrium profiles from relaxing away from their experimental shapes. These sources subtract out the azimuthal averages ($m = 0$ component of the density and temperature

fluctuations) at each time step. The azimuthal average of the potential ϕ is allowed to evolve in the simulation, allowing zonal flows to arise. The parallel current, which is often found explicitly in these equations is replaced here by $J_\parallel = -N_0 v_{\parallel e}$.

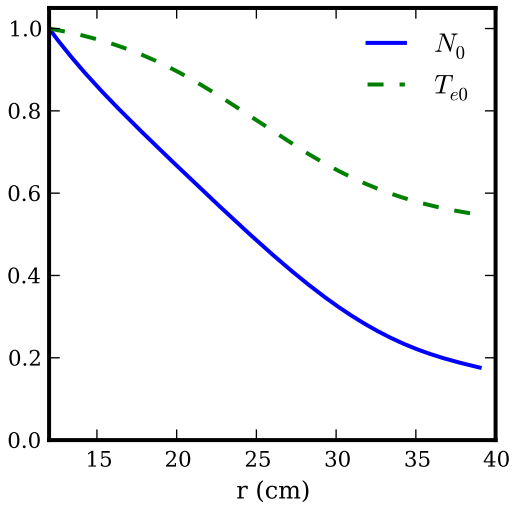

FIG. 1. The profiles of density N_0 and electron temperature T_{e0} used in the simulations normalized to their peak values of 2.86×10^{12} cm^{-3} and 6 eV, respectively.

Some basic statistical properties of the density fluctuations of the simulation are shown in Fig. 2 and are compared to the corresponding results from the experiment on which this simulation is based. The simulation reproduces these characteristics of experimental measurements with rather good qualitative and quantitative accuracy.

III. ENERGETICS MACHINERY

In order to perform an energy dynamics analysis on the simulation, expressions for the energy and energy evolution must be derived from equations 1-4. To start, the expression for the normalized energy of the wave fluctuations in the drift wave model is:

$$E = \frac{1}{2}\int_V (N^2 + \frac{3}{2}T_e^2 + \frac{m_e}{m_i}v_{\parallel e}^2 + N_0(\nabla_\perp \phi)^2)dV. \quad (5)$$

The N^2 contribution is the potential energy due to density fluctuations, $\frac{3}{2}T_e^2$ is the electron temperature fluctuation potential energy, $\frac{m_e}{m_i}v_{\parallel e}^2$ is the parallel electron kinetic energy, and

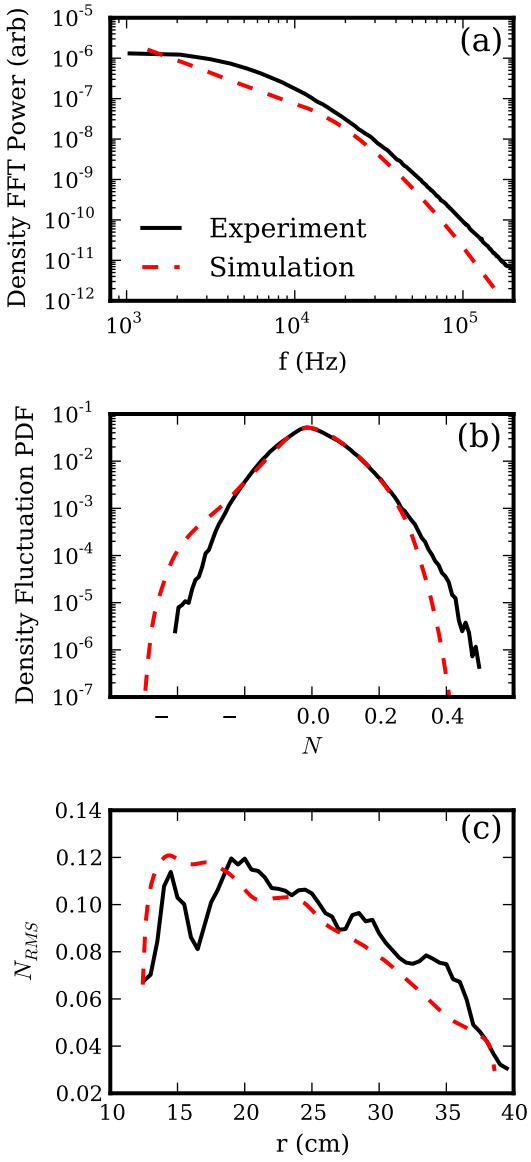

FIG. 2. **a)** The power spectral density of the density fluctuations, showing the results from simulation versus experiment, **b)** the probability distribution function of the density fluctuations, and **c)** the RMS amplitude of the density fluctuations as a function of radius.

$N_0(\nabla_\perp \phi)^2$ is the $E \times B$ perpendicular kinetic energy. These energies are defined in this way so that they are conserved individually by their respective advective nonlinearities, although they are physically relevant as well.

Now, it is most instructive to analyze the spectral energy dynamics rather than the total energy dynamics. To do this, each fluid field $(N, T_e, v_{\parallel e}, \phi)$ at a given time is Fourier decomposed as $F(r,\theta,z) = \sum_{\vec{k}} f_{\vec{k}}(r) e^{i(m\theta + k_z z)}$, where the subscript $\vec{k}$ represents the spectral wavenumbers, (m,n). m is the azimuthal wavenumber while n is the axial integer wavenumber such that $k_z \equiv k_\parallel = 2\pi n / l_z$. Note that the radial direction is not spectrally decomposed because the radial dependence of the profiles and differential operators complicates the analysis. With this, the energy of each Fourier $\vec{k} = (m,n)$ mode is

$$E_{tot}(\vec{k}) = \frac{1}{2}\left\langle |n_{\vec{k}}|^2 + \frac{3}{2}|t_{\vec{k}}|^2 + \frac{m_e}{m_i}|v_{\vec{k}}|^2 + N_0\left|\frac{\partial \phi_{\vec{k}}}{\partial r}\right|^2 + N_0\frac{m^2}{r^2}|\phi_{\vec{k}}|^2 \right\rangle, \tag{6}$$

where the brackets $\langle\rangle$ represent the radial integral: $\int_{r_a}^{r_b} r dr$. The energy evolution for each Fourier mode of each field has the form:

$$\frac{\partial E_j(\vec{k})}{\partial t} = Q_j(\vec{k}) + C_j(\vec{k}) + D_j(\vec{k}) + \sum_{\vec{k}'} T_j(\vec{k},\vec{k}'). \tag{7}$$

The index j stands for each field, (n, t, v, ϕ), and the sum over j gives the total energy evolution. Note that with the conventions used, the symbol n denotes both the axial mode number as well as the Fourier coefficient of the density fluctuation. The differences should be clear in context. The derivation of equation 7 is given in the Appendix along with the full expressions for each of the parts. $T_j(\vec{k},\vec{k}')$ is the nonlinear energy transfer function that comes from the advective nonlinearities. It describes the nonlinear energy transfer rate of modes $\vec{k}' = (m', n')$ and $\vec{k} - \vec{k}' = (m - m', n - n')$ to the mode $\vec{k} = (m,n)$. In other words, a positive value of $T_j(\vec{k},\vec{k}')$ indicates that fluctuations at wavenumber $\vec{k}$ gain energy from gradient fluctuations at wavenumber $\vec{k}'$ and flow fluctuations at wavenumber $\vec{k} - \vec{k}'$. When summed over $\vec{k}'$ as in equation 7, the result is the total nonlinear energy transfer into mode $\vec{k}$. Note that $\sum_{\vec{k},\vec{k}'} T_j(\vec{k},\vec{k}') = 0$ because the nonlinearities conserve energy individually in each of equations 1-4. This is easily proven by the following identity:

$$\int_\Omega q\{p,q\}\, d\Omega = \int_\Omega p\{p,q\}\, d\Omega = 0, \tag{8}$$

which holds when boundary conditions are periodic or zero value as they are in the simulation. The fact that the advective nonlinearities conserve energy means that they can transfer energy between different Fourier modes but they cannot change the energy of

the volume-averaged fluctuations as a whole. Only the linear terms can change the total energy of the fluctuations. Other possible nonlinearities that do not conserve energy are not included in the model equation set or in the simulations for simplicity of the energy analysis. Furthermore, it is convenient for the simulations to employ an energy conserving finite difference scheme for the advective nonlinearities to reflect this analytic property of the equations. However, most common numerical advection schemes do not conserve energy for finite grid spacing. Therefore, an Arakawa advection scheme[36] that conserves energy of the advected quantity is used for the nonlinear advection terms in the simulations.

The linear terms in equations 1-4 do not conserve energy individually or as a whole. The linear terms are broken up into three contributions in Eqn. 7. $D_j(\vec{k})$ represents nonconservative energy dissipation due to collisions, artificial diffusion and viscosity, and the purely dissipative density and temperature sources. Each contribution to $D_j(\vec{k})$ is negative, and the exact expressions are given in the Appendix. $C_j(\vec{k})$ contains the linear terms dubbed "transfer channels"[23]. They are rewritten here:

$$C_n(\vec{k}) = Re\left\{\left\langle -ik_z N_0 v_{\vec{k}} n^*_{\vec{k}}\right\rangle\right\} \tag{9}$$

$$C_v(\vec{k}) = Re\left\{\left\langle -ik_z N_0 n_{\vec{k}} v^*_{\vec{k}} + ik_z N_0 \phi_{\vec{k}} v^*_{\vec{k}} - 1.71 ik_z T_{e0} t_{\vec{k}} v^*_{\vec{k}}\right\rangle\right\} \tag{10}$$

$$C_\phi(\vec{k}) = Re\left\{\left\langle ik_z N_0 v_{\vec{k}} \phi^*_{\vec{k}}\right\rangle\right\} \tag{11}$$

$$C_t(\vec{k}) = Re\left\{\left\langle -1.71 ik_z T_{e0} v_{\vec{k}} t^*_{\vec{k}}\right\rangle\right\} \tag{12}$$

Notice that $C_n(\vec{k}) + C_v(\vec{k}) + C_\phi(\vec{k}) + C_t(\vec{k}) = 0$, which is most clearly seen upon conjugation of $C_v(\vec{k})$ inside the real part operator. This is the reason why these terms are called transfer channels. They represent the transfer between the different types of energy of the different fields ($N, \phi, T_e \leftrightarrow v_{\|e}$), but taken together, they do not create or dissipate total energy from the system. The only energy field transfer in this system occurs through the parallel electron velocity (parallel current) dynamics. There is no direct transfer between the state variables N, ϕ, and T_e. Altogether, the coupling through the parallel current is called the adiabatic response. It is an essential part of both the linear and nonlinear drift wave mechanisms[23,25]. The adiabatic response moves energy from the pressure fluctuations to the perpendicular flow through the parallel current.

Finally, the $Q_j(\vec{k})$ terms represent the nonconservative energy sources. They are rewritten here:

$$Q_n(\vec{k}) = Re\left\{\left\langle -\frac{im}{r}\partial_r N_0 \phi_{\vec{k}} n^*_{\vec{k}}\right\rangle\right\} \tag{13}$$

$$Q_v(\vec{k}) = Re\left\{\left\langle ik_z\frac{N_0^2 - T_{e0}}{N_0} n_{\vec{k}} v^*_{\vec{k}} + ik_z(1-N_0)\phi_{\vec{k}} v^*_{\vec{k}} + 1.71ik_z(T_{e0}-1)t_{\vec{k}} v^*_{\vec{k}}\right\rangle\right\} \tag{14}$$

$$Q_\phi(\vec{k}) = 0 \tag{15}$$

$$Q_t(\vec{k}) = Re\left\{\left\langle -\frac{3}{2}\frac{im}{r}\partial_r T_{e0}\phi_{\vec{k}} t^*_{\vec{k}}\right\rangle\right\} \tag{16}$$

$Q_n(\vec{k})$ is the energy extraction from the equilibrium density profile into the density fluctuations. This term may have either sign depending on the phase relation between $\phi_{\vec{k}}$ and $n_{\vec{k}}$, so it can in fact dissipate fluctuation potential energy from the system as well as create it at each $\vec{k}$. $Q_t(\vec{k})$ is completely analogous to $Q_n(\vec{k})$ but for the temperature rather than the density. $Q_v(\vec{k})$ is parallel kinetic energy extraction or dissipation, which is a rather insignificant term compared to $Q_n(\vec{k})$ and $Q_t(\vec{k})$. The sources of these terms are the equilibrium gradients, which is evident because if the profiles were flat ($N_0 = T_{e0} = 1$), all $Q(\vec{k})$ would vanish. Moreover, the particular normalization of equations 1-4 combined with the choice of energy definition (equation 5) causes the non-zero $Q_v(\vec{k})$, which again is quite insignificant.

IV. NONLINEAR ENERGY DYNAMICS

A. Energy Spectra

Figure 3 shows the time evolution of the total energy of the fluctuations. The simulation starts with a random initial perturbation, and the fluctuations grow exponentially due to the linear drift wave instability until the energy level reaches about 0.05. Then, the nonlinear instability takes over and the fluctuation energy continues to grow until reaching saturation. All analysis shown below is done by time averaging over the saturated (turbulent) stage. The turbulent spectral energy, defined in equation 6 is shown in Fig. 4. The energy is broken up into its different types (e.g. perpendicular kinetic energy: E_ϕ). There are a few clear nonlinear properties seen in these figures. The first is that the energy is located in different spectral regions for the different energy types. This has to be a nonlinear effect because